


Assessment of a PLL-ASMO position/speed estimator for sensor-less control of rotor-tied DFIG (RDFIG)

Mwana Wa Kalaga Mbukani¹  | Nkosinathi Gule² 

¹Department of Electrical, Electronic and Computer Engineering, University of Pretoria, Pretoria, South Africa

²Department of Electrical and Electronic Engineering, Stellenbosch University, Matieland, South Africa

Correspondence

Mwana Wa Kalaga Mbukani, Department of Electrical, Electronic and Computer Engineering, University of Pretoria, Pretoria, South Africa.
Email: mwanawakalaga.mbukani@up.ac.za

Funding information

National Research Foundation of South Africa, Grant/Award Number: 120728

Abstract

In this paper, an adaptive sliding mode observer (ASMO) associated with a phase locked loop (PLL) is assessed for the sensor-less control of a rotor-tied doubly-fed induction generator (RDFIG). In the proposed PLL-ASMO estimator, the ASMO utilizes the stator current, the stator voltage, and the back electromotive force (EMF) as state variables. The proposed ASMO is used in order to estimate the back-EMF from which the slip position/speed is extracted using a PLL. The design of the ASMO gains is based on the Lyapunov stability criteria to ensure the convergence of the proposed observer in a finite time. Therefore, the main contribution of this paper is to propose a PLL-based ASMO estimator that aims to improve the estimation by reducing the chattering effect. A comparative study between the standard PLL-SMO estimator and the PLL-ASMO estimator is presented. Also, For the first time, an adaptive sliding mode observer is used for the sensor-less control of a RDFIG. The performance of the proposed sensor-less control strategy is validated through simulation and experimental measurements under various operating conditions. Furthermore, the estimator is shown to be robust to machine parameter variation.

1 | INTRODUCTION

In the last few decades, there has been a sharp increase in wind turbine generation worldwide. The doubly-fed induction generator is one of the most popular wind turbine generators mainly because of its use of a partially rated power converter [1–3]. Additionally, its ability to have a high low voltage capabilities. To improve the performance of the DFIG, the rotor-tied DFIG (RDFIG) was introduced by ref. [4]. In the RDFIG configuration, the rotor winding is directly connected to the grid while the stator is connected to the back-to-back converter. The RDFIG has been shown to possess better performance when compared to the conventional DFIG [4, 5]. Furthermore, it has been shown that the RDFIG is smaller in volume as compared to the conventional DFIG for the same power rating [4]. The standard vector control of the RDFIG system is discussed in ref. [6].

Similar to conventional DFIGs, the vector control of the RDFIG relies on accurate and reliable speed measurements as it uses the dq -transformation. In harsh environments, the

failure of the mechanical speed encoder could lead to the failure of the overall control system and that of other components of the DFIG/RDFIG system [7]. The cost and the difficulty or installations/maintenance of the mechanical speed measuring devices in DFIGs can be eliminated through the use of sensor-less speed estimation techniques.

In general, position/speed estimation techniques can be classified as saliency-based estimation techniques and model-based estimation methods. In the saliency-based estimation methods, the speed/position of the rotor is estimated through the use of the position of the related inductance under high frequency signal injection [7–9]. Thus, the saliency-based estimation methods are mostly suitable for standstill and start-up operating conditions. The model-based estimation techniques are used to estimate the rotor speed/position based on the machine model at the fundamental frequency and they are mostly used for medium-speed and high-speed applications [10–32]. The model-based estimation techniques are generally grouped into two categories: the open loop calculations and closed loop observers. In the open loop calculations, the state variables of

This is an open access article under the terms of the [Creative Commons Attribution](https://creativecommons.org/licenses/by/4.0/) License, which permits use, distribution and reproduction in any medium, provided the original work is properly cited.

© 2023 The Authors. *The Journal of Engineering* published by John Wiley & Sons Ltd on behalf of The Institution of Engineering and Technology.

the DFIG (back-EMF, stator current, rotor current, or rotor flux) are used as inputs. Using the DFIG model, the state of interests are deduced and then the estimated rotor speed/angle is extracted from the calculated state of interests. In the closed loop observers, both the state variable and the error between the outputs of the plant and that of the observer are input to the observer. The observer gains are designed such that the state variable of the observer converge to their real values from the plant. There are several closed loop observers presented in the literature for the sensor-less control of the DFIG system.

The sliding mode observer (SMO), which is an example of the model-based estimation techniques, is known for its dynamic response and robustness against machine parameter variations. An SMO-based position/speed estimator for the sensor-less control of a DFIG is proposed, simulated, and experimentally validated in refs. [18] and [19]. The proposed SMO utilized the stator flux and the rotor current as state variables. In ref. [25], a phase-locked loop (PLL)-based SMO position/speed estimator for the sensor-less control of a RDFIG is proposed. The performance of the proposed PLL estimator was validated through simulations and it was shown that the inclusion of a judgment function in the PLL allows for the estimator to operate under all operating conditions [25]. In ref. [32], it was shown that the use of the PLL, in the sensor-less control of an RDFIG, mitigates the lagging effect introduced by the low pass filter. In ref. [30], it was shown that the use of a high order sliding mode observer (HOSMO) helps in improving the performance of the position/speed estimator while also reducing the noise in the estimated signals. Another SMO-based estimator, the super twisting sliding mode observer (STSMO), is proposed for the sensor-less control of the RDFIG in ref. [31], whereby it was shown that the use of the super twisting algorithm (STA) improves the performance of the proposed position/speed estimator.

In refs. [25, 30–32], in the implementation of the SMO-based estimators, the estimated rotor speed is calculated using the arc-tangent function. The noise and the harmonics created by the switching of the sliding mode functions might alter the estimation performance. To reduce the chattering effect often associated with SMO-based positions/speed estimators, adaptation approaches for tuning the control gains of an adaptive SMO (ASMO) based sensor-less control method for permanent magnet synchronous machine (PMSM) are presented in ref. [33]. It was shown that the ASMO is superior to the standard SMO when chattering and disturbance response is considered. In ref. [34], an ASMO that aims at robustness, smoothness and fast transient performance of a non-linear system is presented.

In ref. [35], a mathematical model of the rotor-tied DFIG in the rotor-flux reference frame when considering an observer at the stationary reference frame, is presented. The authors also proposed a position sensor-less algorithm, based on simple algebraic equations, for the rotor-tied DFIG system to estimate the rotor position.

In this paper, a PLL-ASMO estimator that reduces the chattering effect for the sensor-less control of a RDFIG system is proposed. The design of the adaptive control gains is also discussed and the stability analysis of the ASMO is presented.

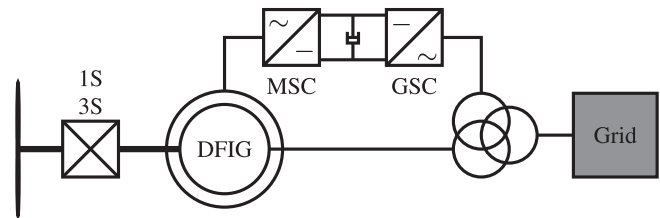


FIGURE 1 Schematic of the WECS-based RDFIG.

Finally, the design of the PLL estimator is presented. Compared to the SMOs proposed in refs. [30–32] for the sensor-less control of a RDFIG, the proposed ASMO leads to the reduction of the noise that is introduced by the switching function. This is achieved through the use of an adaptive sliding mode function. A comparative study is conducted in order to demonstrate the advantage of the proposed ASMO over the standard SMO. Therefore, the contributions of this paper can be summarized as follows:

- The design of an PLL-ASMO estimator for the sensor-less control of a RDFIG.
- The experimental validation of the PLL-ASMO estimator on a RDFIG.
- Although under machine parameter variations there is an increase in noise (in the estimated speed/position) from the proposed PLL-ASMO estimator (which is common for the estimation techniques based on SMO), its robustness is validated experimentally under machine parameter (L_s and R_s) variations in different operating conditions related to a RDFIG.
- A comparative study is conducted between the ASMO and the standard SMO (with constant SMO gains). It has been demonstrated that the use of the ASMO is shown to reduce the noise of the estimated speed/position compared to the standard SMO during change in the stator current magnitude.

The rest of the paper is organized as follows; in Section 2, the mathematical model of the RDFIG is presented while in Section 4 the proposed sensor-less control strategy is given. In Section 3, the design of the PLL-ASMO estimator is presented and discussed. Simulation and experimental results for validating the proposed PLL-ASMO estimator for the sensor-less control of RDFIG are discussed in Section 5. Conclusions are drawn from the analysis of the results and are presented in Section 6.

2 | RDFIG SYSTEM MODEL

A RDFIG-based wind energy conversion system (WECS) is shown in Figure 1. In the RDFIG configuration, the stator winding is connected to the grid through the back-to-back converter while the rotor winding is directly connected to grid. The general operation of the RDFIG is presented in refs. [4] and [36].

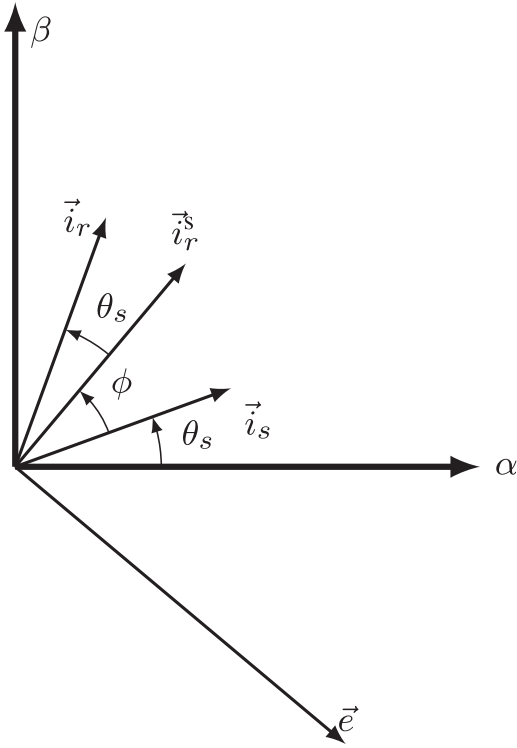


FIGURE 2 Vector diagram of the current space vectors.

In the stationary reference frame, the RDFIG model can be expressed as,

$$\begin{cases} \frac{di_{s\alpha}}{dt} = \frac{1}{L_s} v_{s\alpha} - \frac{R_s}{L_s} i_{s\alpha} + \omega_r i_{s\beta} + e_\alpha \\ \frac{di_{s\beta}}{dt} = \frac{1}{L_s} v_{s\beta} - \frac{R_s}{L_s} i_{s\beta} - \omega_r i_{s\alpha} + e_\beta \\ e_\alpha = \frac{L_m}{L_s} |\vec{i}_r^s| \omega_g \sin \theta \\ e_\beta = -\frac{L_m}{L_s} |\vec{i}_r^s| \omega_g \cos \theta \end{cases} \quad (1)$$

where $i_{s\alpha}$ and $i_{s\beta}$ represents the α -axis and the β -axis stator currents, respectively; $v_{s\alpha}$ and $v_{s\beta}$ represents the α -axis and the β -axis stator voltages, respectively; e_α and e_β represents the α -axis and the β -axis back-EMFs, respectively; ω_g is the rotor flux angular speed; ω_r is the electric rotor angular speed; and, $\theta = \theta_s + \phi$, where θ_s is the slip angle and ϕ is the phase angle of the stator current in the slip reference frame; L_m , L_s , L_r represent the magnetizing, stator and rotor inductances, respectively. The slip speed, ω_s , can then be defined as $\omega_s = \omega_g + \omega_r$. In Equation (1), $|\vec{i}_r^s|$ is the magnitude of the stator current space vector in the slip reference frame. The current vector position diagram is shown in Figure 2.

Note that in Equation (1), the back-EMF space vector (e_α and e_β) contains the slip angle in its expression. Therefore, the slip angle information and that of the slip speed can be extracted

from estimated values of the back-EMFs in the stationary reference frame.

The mechanical dynamic equation on the RDFIG is expressed as,

$$J \frac{d\omega_r}{P dt} = \tau_e - \tau_m, \quad (2)$$

where τ_e is the electromagnetic torque; J is the inertia; τ_m is the mechanical torque at the shaft of the RDFIG while P is the pole pairs, respectively.

3 | PLL-ASMO ESTIMATOR

An adaptive sliding mode observer (ASMO) for the sensor-less control of the RDFIG-based WECS is proposed in this section. The Lyapunov stability criteria is utilized in the design of the adaptive control gains to ensure stability. Furthermore, the design of the PLL is also discussed.

3.1 | ASMO

An ASMO that can be used for the RDFIG sensor-less control is presented here. The aim of the proposed ASMO is to estimate the back-EMFs which includes the information of the slip speed/angle as shown in Equation (1). Based on the RDFIG model given in Equation (1), the stator current observer can be written as

$$\begin{cases} \frac{d\hat{i}_{s\alpha}}{dt} = \frac{1}{L_s} v_{s\alpha}^* - \frac{R_s}{L_s} \hat{i}_{s\alpha} + \hat{\omega}_r i_{s\beta} + K(t) \text{sgn}(\tilde{i}_{s\alpha}) \\ \frac{d\hat{i}_{s\beta}}{dt} = \frac{1}{L_s} v_{s\beta}^* - \frac{R_s}{L_s} \hat{i}_{s\beta} - \hat{\omega}_r i_{s\alpha} + K(t) \text{sgn}(\tilde{i}_{s\beta}) \end{cases}, \quad (3)$$

where (sgn) represents the signum function while ($\hat{\cdot}$) denotes the estimated values. The superscript, (*), denotes the reference value and $K(t)$ represents the adaptive gain. the superscript, ($\tilde{\cdot}$), represents the difference between the actual and the estimated values.

The estimation error of the stator current observer can be determined by subtracting Equation (3) from Equation (1) and with the assumption that the reference stator voltage is the same as the actual stator voltage, that is,

$$\begin{cases} \frac{d\tilde{i}_{s\alpha}}{dt} = \tilde{\omega}_r i_{s\beta} - \frac{R_s}{L_s} \tilde{i}_{s\alpha} + e_\alpha - K(t) \text{sgn}(\tilde{i}_{s\alpha}) \\ \frac{d\tilde{i}_{s\beta}}{dt} = -\tilde{\omega}_r i_{s\alpha} - \frac{R_s}{L_s} \tilde{i}_{s\beta} + e_\beta - K(t) \text{sgn}(\tilde{i}_{s\beta}) \end{cases}. \quad (4)$$

The ideal adaptive gain, $K(t)$, is defined as

$$K(t) = c \int_{t_1}^{t_2} |S| d\tau. \quad (5)$$

In Equation (5), t_1 and t_2 are time variables; c is a positive constant and,

$$|S| = \sqrt{\tilde{i}_{s\beta}^2 + \tilde{i}_{s\alpha}^2}. \quad (6)$$

$K(t)$ can be designed using the Lyapunov stability criteria, and this guarantees the convergence of the ASMO in a finite time. If V is assumed as Lyapunov function, then V is stable according to the Lyapunov stability criteria if the conditions,

$$\begin{cases} V > 0 \\ \frac{dV}{dt} < 0 \end{cases}, \quad (7)$$

are satisfied. In this paper, the Lyapunov function, V , is chosen as

$$V = \frac{1}{2}(\tilde{i}_{s\beta}^2 + \tilde{i}_{s\alpha}^2) + \frac{1}{2}(\bar{K} - K(t))^2, \quad (8)$$

where the superscript ($\tilde{}$) denotes that a variable is bounded and $\bar{K} = \max(K(t))$.

It can be observed, from Equation (8), that V is positive definite. Then, from Equations (4) and (8),

$$\begin{aligned} \frac{dV}{dt} = & -\frac{R_s}{L_s}(\tilde{i}_{s\alpha}^2 + \tilde{i}_{s\beta}^2) + \tilde{i}_{s\alpha}[-K(t)\text{sgn}(\tilde{i}_{s\alpha}) + \tilde{\omega}_r i_{s\beta} + e_\alpha] \\ & + \tilde{i}_{s\beta}[-K(t)\text{sgn}(\tilde{i}_{s\beta}) - \tilde{\omega}_r i_{s\alpha} + e_\beta] \\ & - \sqrt{\tilde{i}_{s\alpha}^2 + \tilde{i}_{s\beta}^2} c(\bar{K} - K(t)) \leq 0. \end{aligned} \quad (9)$$

If the estimation is assumed accurate, that is,

$$\tilde{\omega}_r \approx 0, \quad (10)$$

and, also,

$$K(t) > \max(e_\alpha, e_\beta). \quad (11)$$

then the second and third terms in Equation (9) will always be negative. The fourth term is negative because c is a positive constant as indicated in Equation (5). Thus, the Lyapunov stability criteria is fulfilled as all the terms are negative. From Equation (11), $K(t)$ is chosen large enough so that the Lyapunov stability criteria is satisfied. In this paper the sliding surface, S , is chosen as,

$$\frac{dS}{dt} = 0 \text{ and } S = 0, \quad (12)$$

where S , is commonly defined as

$$S = \begin{bmatrix} \tilde{i}_{s\alpha} \\ \tilde{i}_{s\beta} \end{bmatrix}. \quad (13)$$

Substituting Equations (13), (10), (11), and (12) into Equation (4) gives the estimated back-EMF as

$$\begin{bmatrix} \hat{e}_\alpha \\ \hat{e}_\beta \end{bmatrix} = K(t) \begin{bmatrix} \text{sgn}(\tilde{i}_{s\alpha}) \\ \text{sgn}(\tilde{i}_{s\beta}) \end{bmatrix}. \quad (14)$$

3.2 | Design of the ASMO gains

The expression in Equation (4) can be rewritten as

$$\dot{S} = Y - \eta u, \quad (15)$$

where

$$u = K(t)\text{sgn}(S), \quad (16)$$

and Y is given by

$$Y = \begin{bmatrix} -\frac{R_s}{L_s}\tilde{i}_{s\beta} + \tilde{\omega}_r i_{s\beta} + e_\alpha \\ -\frac{R_s}{L_s}\tilde{i}_{s\alpha} - \tilde{\omega}_r i_{s\alpha} + e_\beta \end{bmatrix}. \quad (17)$$

and $\eta = 1$. The gains of the ASMO are designed such that the system trajectories converges to the designated sliding surface in a finite time.

Substituting Equation (16) into Equation (15) yields,

$$\dot{S} = Y - \eta K(t)\text{sgn}(S). \quad (18)$$

Substituting Equation (12) into Equation (18) yields,

$$K(t) \geq \frac{Y\text{sgn}(S)}{\eta} + \psi, \quad (19)$$

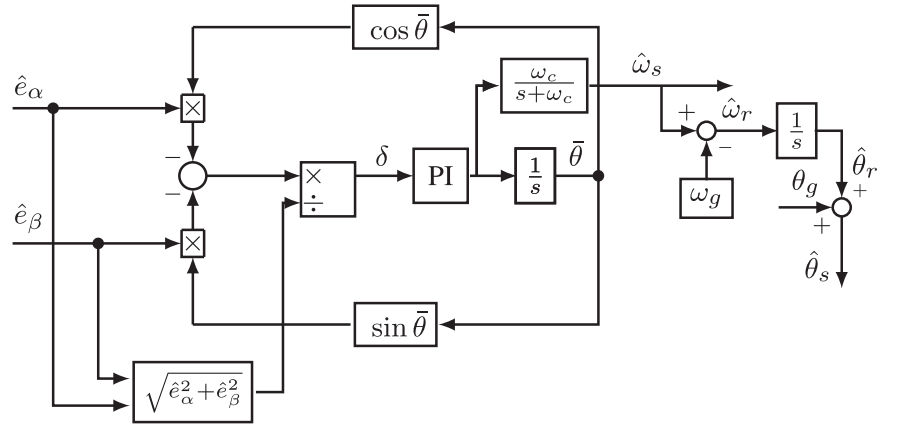
where $\psi > 0$ is small.

The adaptive gain as defined in Equation (5) has a major drawback. Such an adaptive law will continue to increase even if the system trajectory has reached the sliding surface. Therefore, $K(t)$ can become unbounded and this may lead to the instability of the ASMO. Also, the constant increase of $K(t)$ results to more chatter on the estimated signal. To counter these drawbacks, ref. [34], proposed an adaptive law that includes an exponential term which reduces the value of c . The exponential term disappears when the sliding surface is reached by the system trajectory. The adaptive law proposed in ref. [34], can be used with the ASMO proposed in this paper and is given by,

$$K(t) = b \int_{t_1}^{t_2} |S| d\tau + \sigma_0 (e^{\sigma_1 |S|^r} - 1), \quad (20)$$

where b , σ_0 , σ_1 , and r are strictly positive integers. In Equation (20), the extra gain is provided by the exponential term when

FIGURE 3 Schematic diagram of the slip speed/angle estimator.



the system trajectory is far from the desired sliding surface. In the case of a disturbance, the exponential term will ensure that the system trajectory quickly returns to the desired sliding surface. Once the system trajectory reaches the sliding surface, the exponential term will disappear. Thus, the chattering effect will be reduced since the steady state adaptive gain will be small.

The steps for the design of the adaptive law presented in Equation (20) are explained in ref. [34]. A large value of r will result in both the reduction of the response time and the improvement of the accuracy. A proper design of σ_0 , σ_1 , and r will reduce the chattering while providing high accuracy and low response time. The parameters in Equation (20) are chosen in such a way that the expression in Equation (19) is fulfilled. In this way, the parameters of $K(t)$ are chosen so that $K(t)$ is greater than the back-EMF at steady state. The values of the parameters of the adaptive law are listed in Table 2.

3.3 | PLL estimator

To improve the estimation performance, a PLL estimator designed in refs. [25] and [37] is used. The PLL estimator is used for the extraction of the slip speed/angle from the estimated α -axis and β -axis back-EMFs (\hat{e}_α and \hat{e}_β). In Equation (1), it was shown that the α -axis and β -axis back-EMFs include the slip angle. The schematic of the PLL estimator is displayed in Figure 3 whereby the slip angle/speed is estimated using the sine function. From Figure 3, the error between the estimated slip angle and the tracked slip angle is given by

$$\delta = \frac{\omega_g L_m |\vec{i}_r^*|}{\sqrt{\hat{e}_\alpha^2 + \hat{e}_\beta^2}} \left(-\cos \hat{\theta} \sin \bar{\theta} + \sin \hat{\theta} \cos \bar{\theta} \right) = \sin(\hat{\theta} - \bar{\theta}), \quad (21)$$

where the superscript ($\bar{\cdot}$) refers to the tracking value. The error, δ , is negligible, therefore,

$$\delta \approx \hat{\theta} - \bar{\theta}. \quad (22)$$

The PI controller's goal is to reduce the error, δ , to zero such that $\hat{\theta} = \bar{\theta}$.

From Figure 3, the estimated rotor speed is given by

$$\hat{\omega}_r = \hat{\omega}_s - \omega_g, \quad (23)$$

and the estimated slip angle is given by

$$\hat{\theta}_s = \hat{\theta}_r + \theta_g. \quad (24)$$

The PI gains can be designed following the design process shown below.

3.3.1 | Design of the PLL gains

The PLL estimator gains are designed based on the consideration of the anti disturbance performance [37]. Using small signal analysis shown in Equations (21)–(22) together with the relationship between the estimated slip speed and the estimated slip angle which is given by

$$\hat{\omega}_s = \frac{d\hat{\theta}_s}{dt}. \quad (25)$$

Using small signal analysis, the block diagram of the control loop of the PLL estimator is shown in Figure 5. The closed loop PLL's transfer function is given by,

$$\frac{\hat{\theta}}{\bar{\theta}} = \frac{K_p s + K_i}{s^2 + K_p s + K_i} \quad (26)$$

It is important to note that the filter with a cut-off frequency ω_c of the first order filter shown in Figure 3, is not included in the design of the PLL gains. Hence, the choice of ω_c must be large enough to reduce delay that can affect the estimation performance of the PLL-ASMO estimator. The cut-off frequency of the first order filter, ω_c , is chosen to be $2\pi(100)$ rad/s. The schematic of the proposed PLL-ASMO estimator is shown in Figure 4.

As previously stated, the PI gains are designed using the pole placement method such that $K_p = 2\beta$ and $K_i = \beta^2$. β is calculated based on the anti-disturbance performance. The estimated

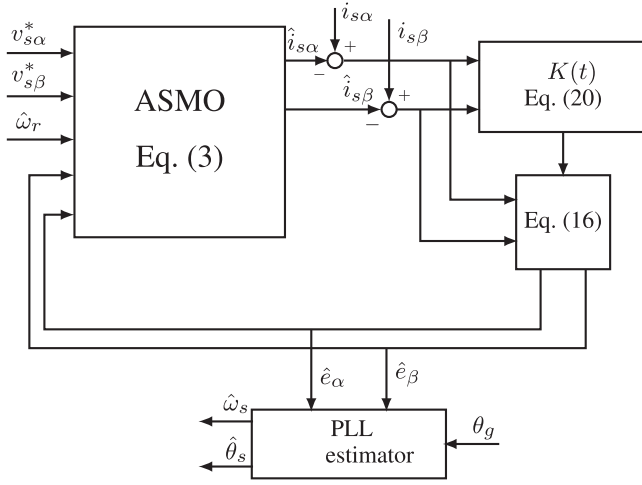


FIGURE 4 Schematic diagram of the proposed PLL-ASMO estimator.

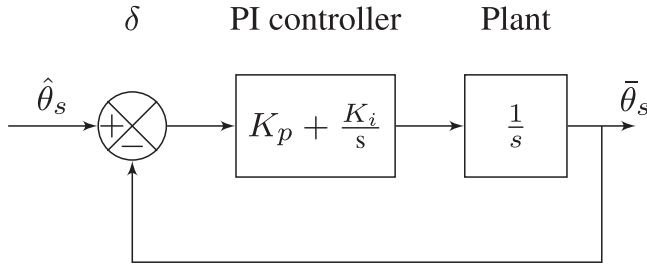


FIGURE 5 Block diagram of PLL estimator.

slip speed and the estimated acceleration are described by,

$$\begin{cases} \dot{\hat{\theta}}_s = \hat{\omega}_s \\ \dot{\hat{\omega}}_s = \phi \end{cases}, \quad (27)$$

where ϕ is the acceleration of the rotor of the RDFIG, as the grid angular frequency ω_g is constant. The superscript $\dot{\cdot}$ denotes the derivative of a variable with respect to the time. Based on the mechanical equation of the RDFIG in Equation (2), the expression of the rotor acceleration is given by

$$\phi = \frac{P\Delta\tau}{J}, \quad (28)$$

where $\Delta\tau$ is the torque change. The expression of the tracking slip speed and tracking slip acceleration are described by

$$\begin{cases} \dot{\hat{\theta}}_s = \hat{\omega}_s + K_p\epsilon \\ \dot{\hat{\omega}}_s = K_i\epsilon \end{cases}, \quad (29)$$

Subtracting Equation (29) from Equation (27), yields

$$\begin{cases} \dot{\hat{\theta}}_s - \dot{\hat{\theta}}_s = \hat{\omega}_s - \hat{\omega}_s - K_p\epsilon \\ \dot{\hat{\omega}}_s - \dot{\hat{\omega}}_s = \phi - K_i\epsilon \end{cases}, \quad (30)$$

Assuming that $\dot{\hat{\theta}}_s - \dot{\hat{\theta}}_s = 0$ and $\dot{\hat{\omega}}_s - \dot{\hat{\omega}}_s = 0$, and considering that that $K_p = 2\beta$ and $K_i = \beta^2$ as stated previously, the expression in Equation (30) becomes

$$\begin{cases} \hat{\omega}_s - \hat{\omega}_s = \frac{2\phi}{\beta} \\ \epsilon = \frac{\phi}{\beta^2} \end{cases}, \quad (31)$$

Hence, from Equation (31) β is given by

$$\beta = \sqrt{\frac{\phi}{\epsilon_{\max}}}, \quad (32)$$

where ϵ_{\max} is the maximum value of the slip position error. Also, it can be seen from Equation (31), that with higher values of β , the error between the estimated and tracking slip angular speed can be reduced. A good rule of thumb is to take $\epsilon_{\max} = \frac{\pi}{12}$. The machine data are also used to determine the maximum acceleration. Hence, β can be calculated. The PLL gains are therefore deduced. Hence, the tuned PLL gains were $K_p = 240$ and $K_i = 14,400$.

4 | RDFIG SENSOR-LESS CONTROL

In Figure 6, a schematic of the proposed sensor-less control strategy, consisting of a stator side control scheme and a grid side (rotor side) control scheme, is displayed. As shown, both control schemes employ a cascaded structure that includes PI controllers. The control schemes are implemented in the synchronous $dq0$ -reference frame. The stator quantities are transformed into the synchronous reference frame using the estimated slip angle, $\hat{\theta}_s$ calculated from the PLL-ASMO estimator.

In this paper, the stator side control scheme which regulates the rotor speed is of interest. In the stator side control scheme, the outer control loop aims at the regulation of the rotor speed while the inner control loop is devoted to the current control.

In the outer control loop, the reference rotor speed, ω_r^* , is compared with the estimated control speed (calculated from the PLL-ASMO estimator), $\hat{\omega}_r$, to provide the input of the outer PI. The output of the outer PI is the reference d -axis stator current, i_{sd}^* , in the inner control loop. In the inner control loop, the error between the reference d -axis stator current (from the outer control loop) and the measured d -axis stator current, i_{sd} . The reference q -axis stator current, $i_{sq}^* = 0$, is set to zero so that the reactive power comes entirely from the grid (rotor side). The

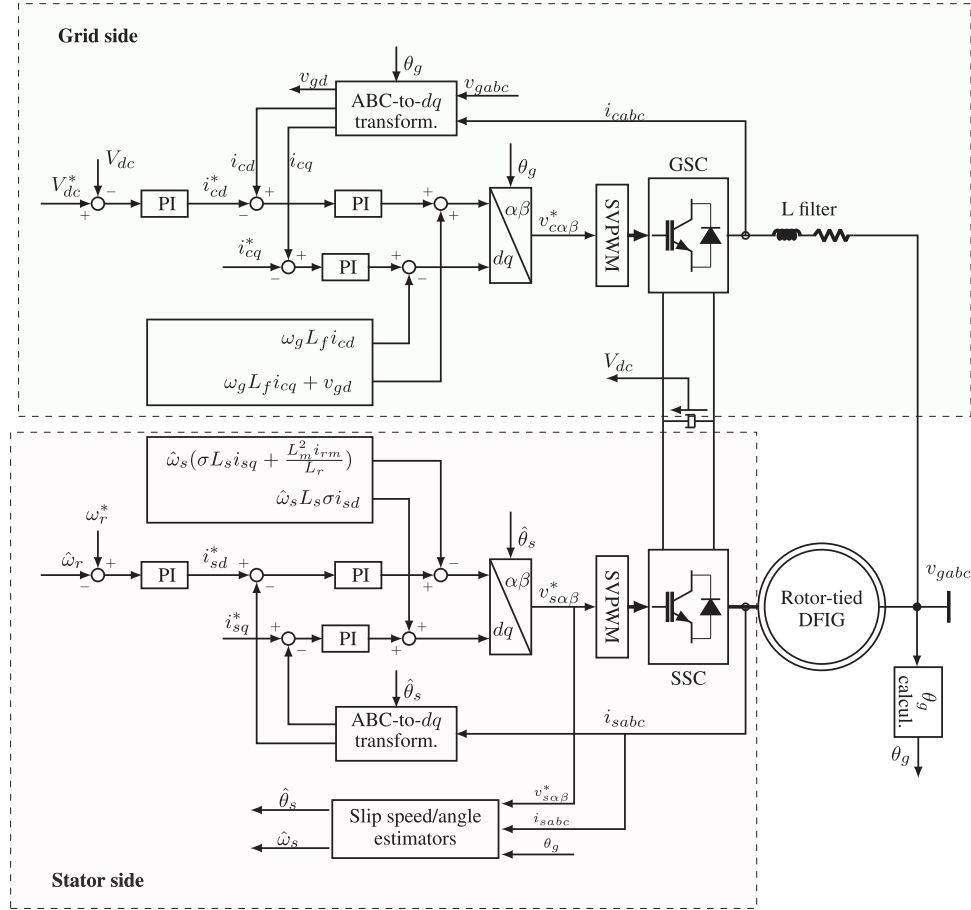


FIGURE 6 The proposed RDFIG sensor-less control strategy with the PLL-ASMO estimator.

reference q -axis stator current is compared to the measured q -axis stator current, i_{sq} , to provide the error to be input to the PI controller. The outputs of the PI controllers are added to the compensation terms in order to provide the actuating signals for the power converter.

A standard grid side control scheme is adopted to maintain the DC-link voltage constant in order to allow for bidirectional power flow in the back-to-back power converters.

5 | RESULTS AND DISCUSSIONS

The proposed PLL-ASMO estimator for RDFIG sensor-less control is validated through simulations and practical measurements, with the results presented in this section. Simulations were performed in MATLAB/SIMULINK while experiments were conducted on a testbed shown in Figure 9 that include a 5.5-kW custom-designed RDFIG [36], a National Instrument (NI) PXIe-8115 real-time controller, two modified commercially-available three-phase 8.7-kVA SEW power converters and a 22-kW induction motor. In Table 1, the RDFIG machine parameters [36] are given. In Tables 2 and Table 3, the designed parameters of the stator side and grid side control schemes are presented, respectively. Also, in Table 2, the gains of the PLL and ASMO are given.

TABLE 1 Machine parameters [36].

Quantity	Value
Rated power	5.5 kW
Rated stator voltage	390 V
Rated rotor voltage	400 V
DC-link voltage	600 V
Stator resistance	2.15 Ω
Rotor resistance	1.855 Ω
Magnetizing inductance	0.257 H
Rotor inductance,	0.2758 H
Stator inductance	0.2758 H
Inertia	0.0003215 kg m ²
Pole-pairs	2

5.1 | Simulations results

The simulation results demonstrating the robustness of the proposed sensor-less control scheme with the RDFIG under sub-synchronous operating conditions is displayed in Figure 7. For these results, the reference rotor speed is fixed at -188.4 rad/s. At about $t = 0.2$ s, the estimated slip speed, $\hat{\omega}_s$,

TABLE 2 Stator side controller parameters.

Quantity	Value
Inner PI proportional gain	$K_p = 36$
Inner PI integral gain	$K_i = 750$
Outer PI proportional gain	$K_p = 0.21$
Outer PI proportional gain	$K_i = 20$
PLL gains	$K_p = 240$ and $K_i = 14,400$
ASMO gains	$b = 200$ and $\sigma_0 = \sigma_1 = r = 200$

TABLE 3 Grid side parameters.

Quantity	Value
L filter	$R_f = 0.2 \Omega$ and $L_f = 0.009$ H
Converter capacitor	$C = 500 \mu$ F
Inner PI gains	$k_p = 30$ and $k_i = 850$
Outer PI gains	$k_p = 0.73$ and $k_i = 24.3$

is aligned with the measured slip speed, ω_s . The convergence of the slip speed error, $\Delta\omega_s$, to zero can also be observed as expected. Similarly, the actual slip angle and estimated slip angle is also shown to converge, and as shown in the figure, the slip angle error, $\Delta\theta_s$, reduces to zero.

With the RDFIG under super-synchronous operating conditions, the simulation results of the proposed sensor-less control scheme, are displayed in Figure 8. Here, the reference rotor speed, ω_r^* is set to -354.8 rad/s. From top to bottom, the measured and the estimated slip speeds, the slip speed error, the estimated and the measured slip angles and the slip angle error are presented. From Figure 8, a similar performance trend as in Figure 7 can be clearly observed and this shows that the control scheme is robust even when the RDFIG is operating at super-synchronous conditions.

5.2 | Laboratory results

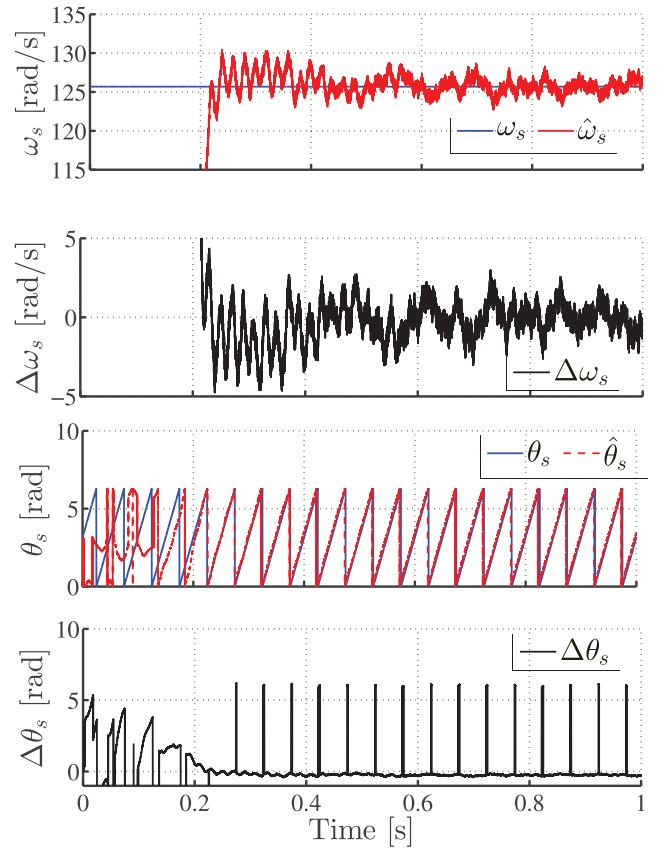
5.2.1 | Grid-side control

The performance of the grid-side control scheme is portrayed in Figure 10. The measured DC-link voltage (V_{dc}) is maintained at 550 V.

5.2.2 | Stator-side control

A GI31 BAUMER incremental encoder is used for actual shaft speed measurement in order to validate the proposed PLL-ASMO speed/position estimator. The switching frequency of the PWM signals used in the converter is set at 5 kHz.

The measurement results showing the performance of the PLL-ASMO speed/position estimator during the sub-synchronous speed operation mode of the RDFIG, are

**FIGURE 7** Simulations results demonstrating the performance of the PLL-ASMO estimator under sub-synchronous operating conditions.

presented in Figure 11, with the RDFIG's speed kept at -188.4 rad/s. It is observed that the actual slip speed and the estimated slip speed converge, that is, the slip speed error is reduced to close to zero. A similar pattern is also observed from the actual and estimated slip angles. Comparing Figures 11 and 7, one can see a similar pattern.

With the RDFIG's speed at -354.8 rad/s, that is, at super-synchronous operating conditions, the performance of the PLL-ASMO speed/position estimator is presented in Figure 12. It is observed that the estimation errors in Figures 12 and 8 have similar patterns as they settle close to zero at steady state and therefore, this further validates the simulation results and shows that the control scheme is robust at super-synchronous conditions.

The performance of the proposed PLL-ASMO estimator under change in the reference rotor speed from super-synchronous to sub-synchronous operating conditions is displayed in Figure 13. From Figure 13, it can be observed that during the speed transition, the maximum slip speed error is 2.5 rad/s. A similar performance is observed in Figure 14 whereby the rotor speed transitions from sub-synchronous to super-synchronous speed.

The performance of the proposed PLL-ASMO estimator during a steady decrease of the rotor speed under inaccurate machine parameters ($1.3L_s$ and $1.3R_s$) is shown in Figure 15 while its performance during a steady increase in rotor speed is

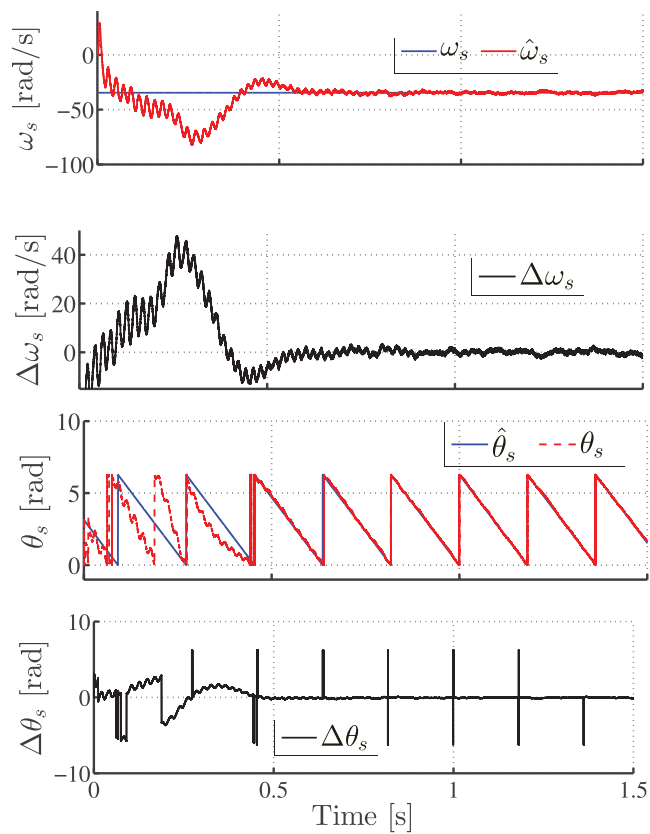


FIGURE 8 Simulation results demonstrating the performance of the PLL-ASMO estimator under super-synchronous operating conditions.

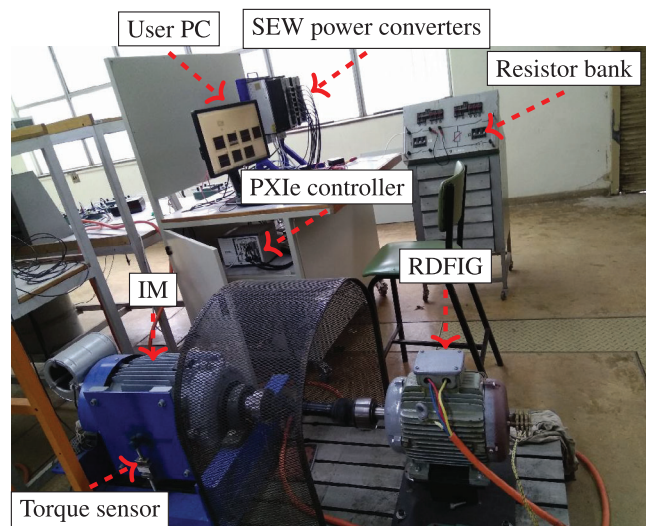


FIGURE 9 A picture of the RDFIG test-bench.

shown in Figure 16. L_s and R_s are chosen for testing the robustness of the system against machine parameters variations they can cause the instability of the all system because they form the plant of the system. Also, the observer depends on the above-mentioned parameters as well.

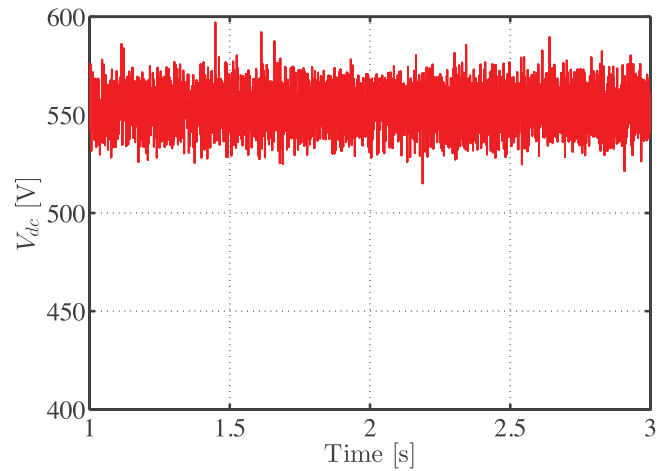


FIGURE 10 Performance of the grid-side controller.

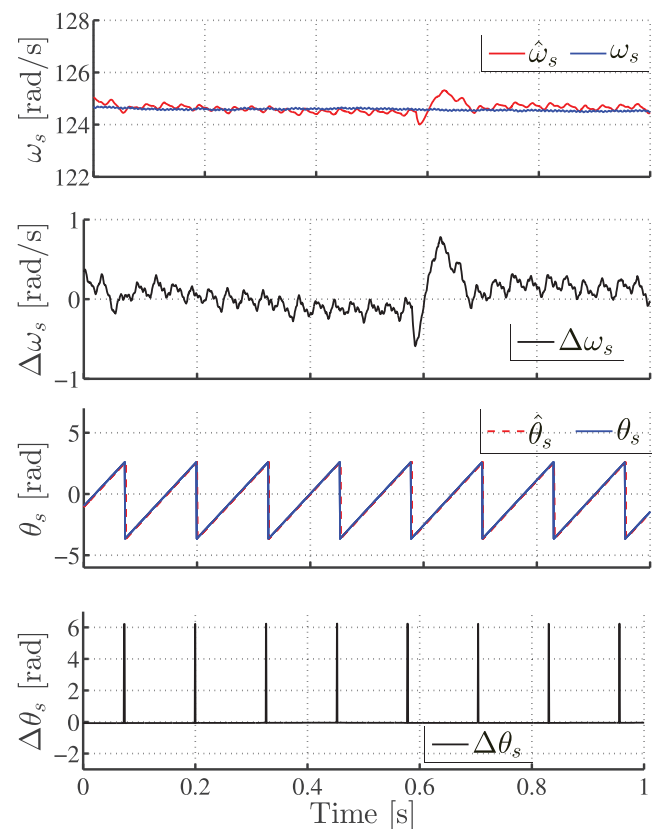


FIGURE 11 Performance of the PLL-ASMO estimator with the RDFIG under sub-synchronous operating conditions.

From Figures 15 and 16, acceptable performance of the estimator can be observed. The inaccurate machine parameters clearly lead to more chattering effect (when comparing Figures 15 and 16 to Figures 13 and 14). The increase in the chatter on the estimated slip speed does not deter the dynamic performance of the PLL-ASMO estimator. Therefore, it has been demonstrated that the proposed PLL-ASMO estimator is immune to parameter variations.

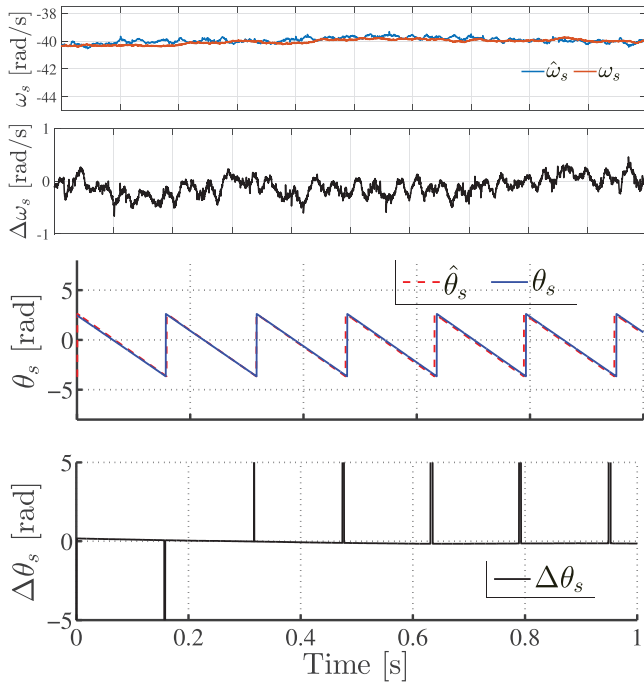


FIGURE 12 Performance of the PLL-ASMO estimator with the RDFIG under super-synchronous operating conditions.

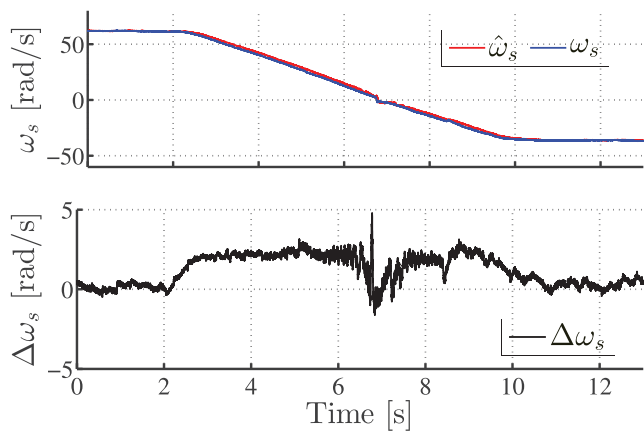


FIGURE 13 The dynamic performance of the PLL-ASMO estimator during speed changes.

The performance of the proposed RDFIG sensor-less controller employing the PLL-ASMO estimator under 30% increase of the stator resistance and the stator inductance combined with the magnitude change of the stator current is shown in Figure 17. In the figure, from top to bottom, the estimated and the measured slip speeds, the slip speed errors, the d -axis stator current and the PLL-ASMO gain are presented. The results displayed in Figure 17 are recorded with the RDFIG speed kept at around 95 rad/s. During steady stator operating condition, one can see that the estimated slip speed converges to the measured slip speed. A change in stator current magnitude occurs at 0.7 s. It can be seen that value of the slip speed error is less than 10 rad/s. In addition, the adaptive gain of the estimator responds automatically at the same instance where there is the

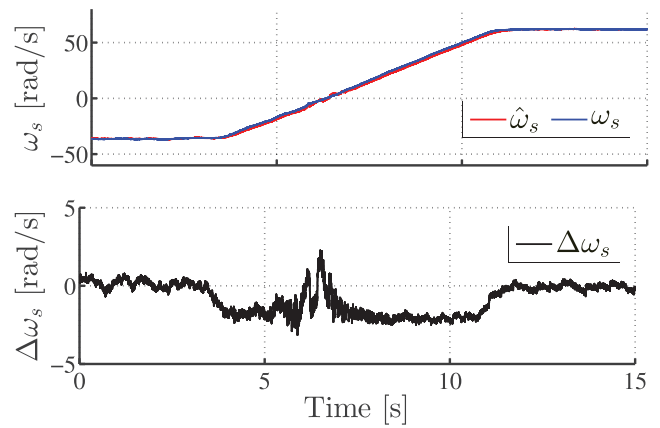


FIGURE 14 The dynamic performance PLL-ASMO estimator during speed transition.

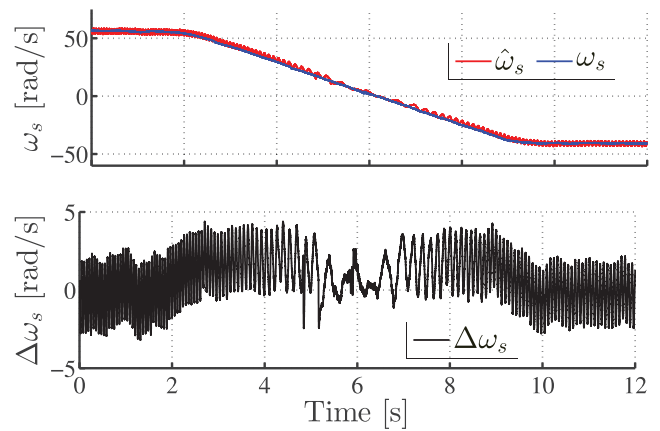


FIGURE 15 The dynamic robustness during rotor speed change with inaccurate machine parameters ($1.3L_s$ and $1.3R_s$).

change in current magnitude. That is, there is a swift response to the disturbance. The estimated slip speed includes spikes as the machine is operating under inaccurate machine parameters. A decrease of stator current magnitude occurs suddenly at $t = 3.4$ s. The same pattern can be observed as the value of the slip speed error is less than 10 rad/s. The adaptive gain automatically adjust in order to cater for the disturbance. Hence, the PLL-ASMO estimator performs reasonably well under machine parameter variation.

The performance of the proposed sensor-less control strategy under a change in speed from sub-synchronous operating conditions to super-synchronous operating conditions and then back to sub-synchronous operating conditions is demonstrated in Figure 18. It is observed that during the transient condition, the absolute values of the slip speed error are less than 4 rad/s. Also, the estimated slip speed is accurately tracking the measured slip speed. When the rotor of the RDFIG reaches synchronous speed ($\omega_s = 0$ rad/s) at $t = 1.35$ s, the three-phase stator currents change from AC to DC as expected for a normal DFIG control system. Also, the change in sequence of the stator currents waveforms from sub-synchronous to super-synchronous operating conditions is clearly demonstrated in the

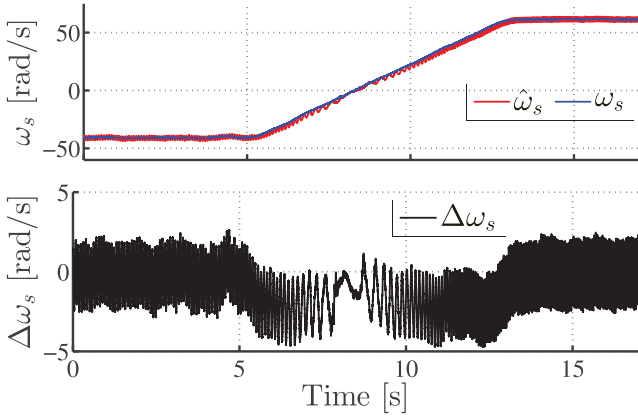


FIGURE 16 The dynamic performance of the PLL-ASMO estimator when the rotor speed changes with inaccurate RDFIG parameters ($1.3L_s$ and $1.3R_s$).

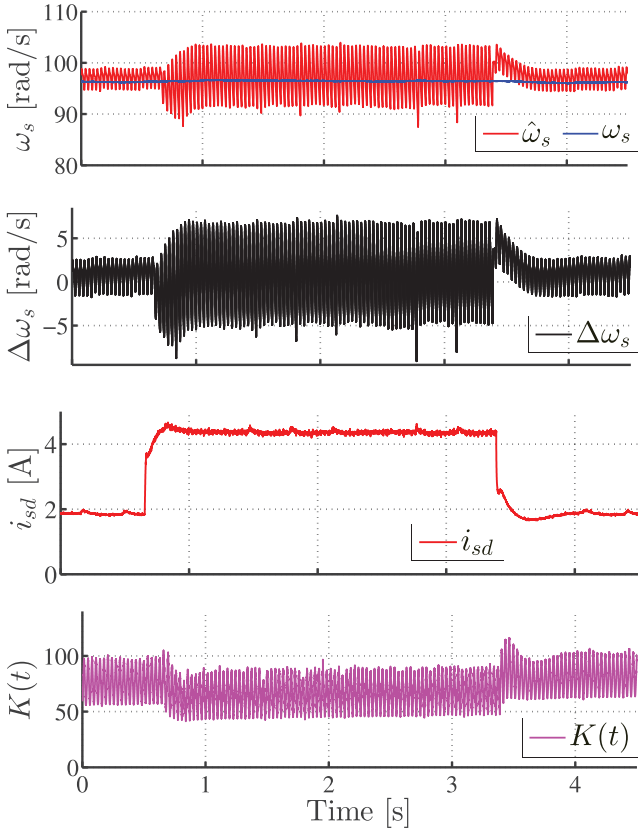


FIGURE 17 Dynamic performance of the PLL-ASMO estimator during sudden stator current magnitude change with inaccurate RDFIG parameters ($1.3L_s$ and $1.3R_s$).

figure. The frequency of the three-phase stator currents is also seen to be proportional to the slip speed.

5.3 | Comparative study

In this section, an experimental comparative study between the PLL-based ASMO estimator and the standard PLL-SMO esti-

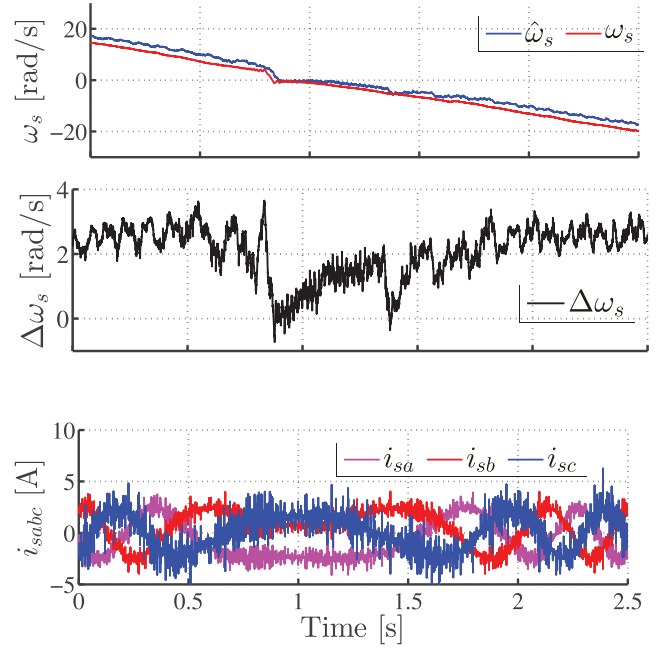
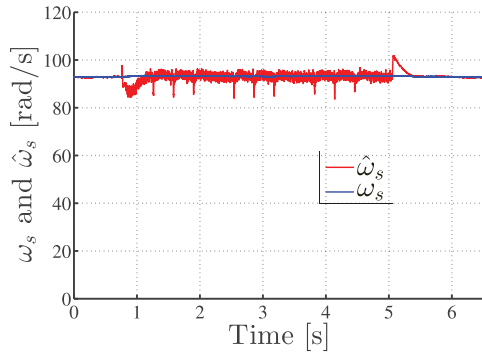


FIGURE 18 Transient performance of the proposed RDFIG PLL-ASMO based sensor-less control.

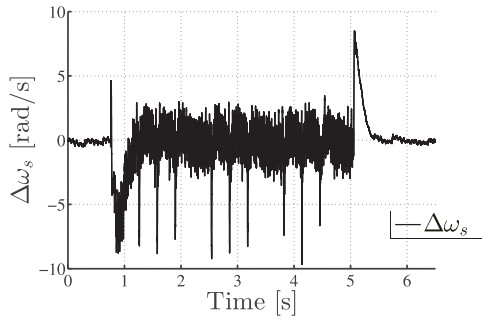
imator is discussed under change in the stator current magnitude (with no change in the machine parameters). The stator current is a variable of interest for the ASMO as the estimated rotor speed is extracted from this variable. Hence, the dynamics of the stator current are of high interest.

In Figures 19 and 20, the proposed control strategy during stator current changes is presented with an adaptive observer gain and a constant gain ($K = 400$), respectively. The constant gain is chosen 400 as this is the minimum gain that guarantee that the system trajectory is met. In this experiment, the RDFIG is rotating at 1050 rpm which is equivalent to about 92 rad/s of slip speed, as shown in Figures 19(c) and 20(a). It can be seen that the actual and estimated slip speed are aligned perfectly during steady operating conditions.

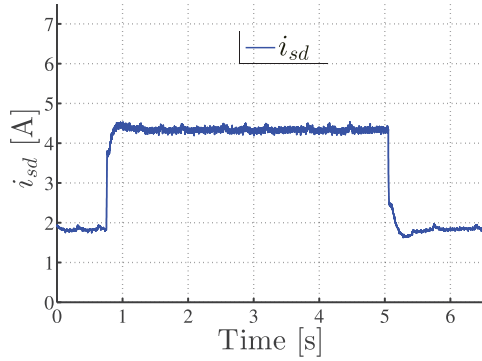
Comparing the performance of the SMO estimator and the ASMO estimator, it can be seen that during the stator current magnitude change at about $t = 0.8$ s a sudden increase in the stator current magnitude as shown in Figures 19(c) and 20(c), the maximum slip speed error for the ASMO estimator is less than $\Delta\omega_s = 10$ rad/s, as shown in Figure 19(b) while that of the SMO estimator is about $\Delta\omega_s = 11$ rad/s, shown in Figure 20(b). Also, during the change, it can be seen that the adaptive gain is adjusted on-line in order to reduce the chattering effect, as it can be seen in Figure 19(d). However, it can be seen that the slip speed waveform includes spikes which are mostly due the fact that the adaptive gain is a function of the sliding surface. Although the ASMO estimator is very sensible to the dynamics of the stator current the spikes in the slip speed waveform does not affect the sensor-less operations. At about $t = 5.2$ s there is a decrease in the current magnitude to its initial value. The adaptive gain is also adjusted on-line, as shown in Figure 19(d).



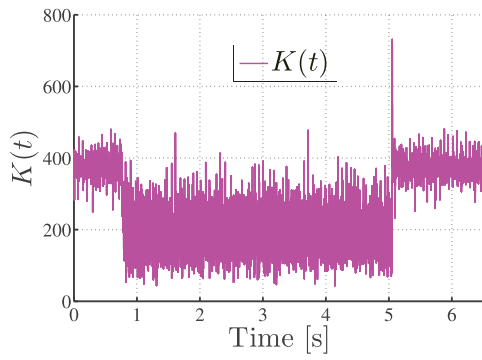
(a)



(b)

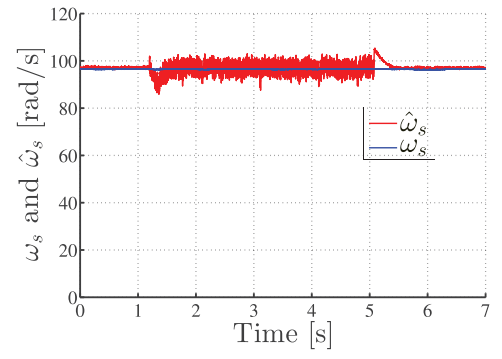


(c)

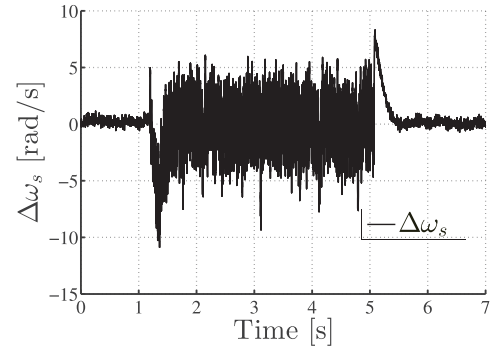


(d)

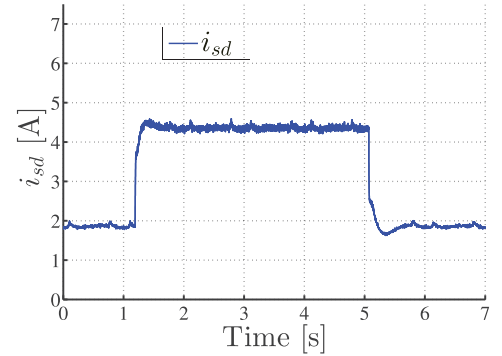
FIGURE 19 The transient performance during change in stator current magnitude: (a) The actual slip speed, ω_s and the estimated slip speed, $\hat{\omega}_s$; (b) The slip speed error, $\Delta\omega_s$; (c) The d -axis stator current, i_{sd} ; and (d) The adaptive gain, $K(t)$.



(a)



(b)



(c)

FIGURE 20 The transient performance: (a) The actual slip speed ω_s and the estimated slip speed $\hat{\omega}_s$; (b) The slip speed error, $\Delta\omega_s$; and (c) the d -axis stator current, i_{sd} .

It can be concluded that the ASMO estimator betters the slip/angle estimation during transient compared to that of the SMO estimator. Hence it improves the accuracy of the slip speed/angle estimation.

6 | CONCLUSION

A PLL-ASMO estimator for the sensor-less control of a grid-connected rotor-tied DFIG systems has been assessed and investigated in this paper. A grid-side converter control strategy aiming at maintaining the DC-link voltage constant was

proposed. The proposed PLL-ASMO estimator is based on the association of the PLL estimator and the ASMO with the aim of improving the performance of the proposed slip speed estimator. Steady state and transient measurement results were presented for operating conditions that are more likely to occur in RDFIG operations. The performance of the proposed control strategy is validated through simulations and experimental tests on a 5.5-kW custom-designed RDFIG. It has been shown that the ASMO helps in reducing the noise (chattering) of the estimated speed/position during standard operating conditions of a 5.5-kW custom-designed RDFIG. Furthermore, the slip speed error from the measurement results is less than 1.5 rad/s with accurate RDFIG parameters (L_s and R_s). With inaccurate RDFIG parameters, the slip speed error is still less than 4 rad/s. Therefore, the PLL-ASMO estimation method is robust. A comparative study between the PLL-ASMO estimator and the PLL-SMO estimator has demonstrated that the PLL-ASMO estimator performs better to the stator current magnitude change with a smaller $\Delta\omega_s$.

NOMENCLATURE

c	a positive constant
e_α	the α -axis back-EMFs
e_β	the β -axis back-EMFs
$i_{s\alpha}$	the α -axis stator currents
$i_{s\beta}$	the β -axis stator currents
J	the inertia
$K(t)$	the adaptive gain
L_m	the magnetizing inductance
L_r	the rotor inductance
L_s	the stator inductance
P	the pole pairs
S	the sliding surface
$v_{s\alpha}$	the α -axis stator voltages
$v_{s\beta}$	the β -axis stator voltages
WECS	Wind Energy conversion system
ϕ	the phase angle of the stator current in the slip reference frame
sgn	the signum function
τ_m	the mechanical torque
θ_s	the slip angle
ω_g	the rotor flux angular speed
ω_r	the electric rotor angular speed
ω_s	the slip speed
$ \vec{i}_r^s $	the magnitude of the stator current space vector in the slip reference frame

AUTHOR CONTRIBUTIONS

Mwana Wa Kalaga Mbukani: Conceptualization, data curation, formal analysis, funding acquisition, investigation, methodology, project administration, software, validation, visualization, writing – original draft, writing – review and editing. Nkosinathi

Gule: Funding acquisition, supervision, validation, writing – review and editing.

CONFLICT OF INTEREST STATEMENT

The authors declare no conflict of interest.

DATA AVAILABILITY STATEMENT

Data is contained within the article.

ORCID

Mwana Wa Kalaga Mbukani  <https://orcid.org/0000-0003-2866-3001>

Nkosinathi Gule  <https://orcid.org/0000-0002-2629-4874>

REFERENCES

- Pena, R., Clare, J.C., Asher, G.M.: Doubly fed induction generator using back-to-back PWM converters and its application to variable wind-energy generation. *IEE Proc. Elect. Power Appl.* 143, 231–241 (1996)
- Muller, S., Deicke, M., Doncker, R.D.: Doubly fed induction generator systems for wind turbines. *IEEE Ind. Appl. Mag.* 8, 26–33 (2002)
- Tazil, M., Kumar, V., Bansal, R.C., Kong, S., Dong, Z.Y., Freites, W., Mathur, H.D.: Three-phase doubly-fed induction generators: an overview. *IET Electr. Power Appl.* 4(2), 75–89 (2010)
- You, M.Y., Lipo, T.A., Kwon, B.L.: Design and analysis of a novel grid-connected to rotor type fed induction machine. *IEEE Trans. Magn.* 48(2), 919–922 (2012)
- David, N., Aliprantis, D.C.: Improved efficiency of DFIG wind energy conversion systems by operating in the rotor-tied configuration. In: *Proceedings of the 2014 International Conference on Electrical Machines (ICEM)*, pp. 189–195. IEEE, Piscataway, NJ (2014)
- Mbukani, M.W.K., Gule, N.: Experimental implementation of the stator-side control of a grid-connected rotor-tied DFIG-based WECS. In: *2018 International Symposium on Power Electronics, Electrical Drives, Automation and Motion (SPEEDAM)*, pp. 895–900. IEEE, Piscataway, NJ (2018)
- Cadenas, R., Pena, R., Alepuz, S., Asher, G.: Overview of control systems for operation of DFIGs in wind energy applications. *IEEE Trans. Ind. Electron.* 60(7), 2776–2798 (2013)
- Reigosa, D.D., Briz, F., Charro, C.B., Di Gioia, A., García, P., Guerrero, J.M.: Sensorless control of doubly fed induction generators based on rotor high-frequency signal injection. *IEEE Trans. Ind. Appl.* 49(6), 2593–2601 (2013)
- Reigosa, D.D., Briz, F., Blanco, C., Guerrero, J.M.: Sensor-less control of doubly fed induction generators based on stator high-frequency signal injection. *IEEE Trans. Ind. Appl.* 50(5), 3382–3391 (2014)
- Morel, L., Godfroid, H., Mirzaian, A., Kauffmann, J.M.: Double-fed induction machine: converter optimisation and field-oriented control without position sensor. *IEE Proc. Elect. Power Appl.* 145(4), 360–368 (1998)
- Harnefors, L., Nee, H.: A general algorithm for speed and position estimation of AC motors. *IEEE Trans. Ind. Electron.* 47(1), 77–83 (2000)
- Olivieri, C., Tursini, M.: A novel PLL scheme for a sensor-less PMSM drive overcoming common speed reversal problems. In: *2012 International Symposium on Power Electronics Power Electronics, Electrical Drives, Automation and Motion*, pp. 1051–1056. IEEE, Piscataway, NJ (2012)
- Zhang, Y., Liu, J.: An improved Q-PLL to overcome the speed Reversal problems in sensor-less PMSM drive. In: *2016 IEEE 8th International Power Electronics and Motion Control Conference (IPEMC-ECCE Asia)*, pp. 1884–1888. IEEE, Piscataway, NJ (2016)
- Benbouzid, M., Beltran, B., Mangel, H., Mamoune, A.: A high-order sliding mode observer for sensor-less control of DFIG-based wind turbines. In: *IECON 2012-8th Annual Conference on IEEE Industrial Electronics Society*, pp. 4288–4292. IEEE, Piscataway, NJ (2012)
- Mbukani, M.W.K., Gule, N.: Implementation of an SMO-based MRAS estimator for sensor-less control of RDFIG systems. In: *2020*

- International Conference on Electrical Machines (ICEM), pp. 1143–1149. IEEE, Piscataway, NJ (2020)
16. Mbukani, M.W.K., Gitau, M.N., Naidoo, R.: An SMC-MRAS speed estimator for sensor-less control of DFIG systems in wind turbine applications. *Energies* 16(6), 2633 (2023). doi:<https://doi.org/10.3390/en16062633>
 17. Mbukani, M.W.K., Gitau, M.N., Naidoo, R., Masike, L.: A torque-based MRAS estimator for position/speed sensor-less control of DFIG systems. 2022 IEEE 1st Industrial Electronics Society Annual On-Line Conference, pp. 1–6. IEEE, Piscataway, NJ (2022)
 18. Wei, C., Zhang, Z., Zeng, J., Qiao, W.: Stator current-based sliding mode observer for sensor-less vector control of doubly-fed induction generators. In: 2015 IEEE Energy Conversion Congress and Exposition (ECCE), pp. 4165–4171. IEEE, Piscataway, NJ (2015)
 19. Wei, C., Qiao, W., Zhao, Y.: Sliding-mode observer-based sensor-less direct power control of DFIGs for wind power applications. In: IEEE Power and Energy Society General Meeting, pp. 1–5. IEEE, Piscataway, NJ (2015)
 20. Zheng, X., Song, R., Li, H.: Full-order terminal sliding mode stator flux observer for DFIG. In: 2016 IEEE 11th Conference on Industrial Electronics and Applications (ICIEA), pp. 299–303. IEEE, Piscataway, NJ (2016)
 21. Yan, Z., Jin, C., Utkin, V.: Sensor-less sliding mode control of induction motors. *IEEE Trans. Ind. Electron.* 47(6), 1286–1297 (2000)
 22. Shen, B., Low, V., Ooi, B.T.: Slip frequency phase lock loop (PLL) for decoupled P-Q control of doubly-fed induction generator (DFIG). In: 30th Annual Conference of IEEE Industrial Electronics Society (IECON), pp. 80–85. IEEE, Piscataway, NJ (2004)
 23. Asha Rani, M.A., Nagamani, C., Ilango, G.S.: An improved rotor PLL (R-PLL) for enhanced operation of doubly fed induction machine. *IEEE Trans. Sustainable Energy* 8(1), 117–125 (2017)
 24. Tshiloz, K., Vilchis-rodriguez, D., Djukanovic, S., Sarma, N., Djurović, S.: Sensorless speed estimation in wound rotor induction machines by spectral search of the stator phase power. *IET Electr. Power Appl.* 10(6), 581–592 (2016)
 25. Kalaga Mbukani, M.W., Gule, N.: Performance analysis of a PLL-based sensor-less control of rotor-tied DFIG systems. In: 2018 IEEE 9th International Symposium on Sensorless Control for Electrical Drives (SLED 2018), pp. 48–53. IEEE, Piscataway, NJ (2018)
 26. Iacchetti, M.F.: Adaptive tuning of the stator inductance in a rotor-current-based MRAS observer for sensorless doubly-fed induction machine drives. *IEEE Trans. Ind. Electron.* 58(10), 4683–4692 (2011)
 27. Lu, L.-Y., Avila, N.F., Chu, C.-C., Yeh, T.-W.: Model reference adaptive back-electromotive-force estimators for sensorless control of grid-connected DFIGs. *IEEE Trans. Ind. Appl.* 54(2), 1701–1711 (2018)
 28. Abdelrahem, M., Hackl, C., Kennel, R.: Sensorless control of doubly-fed induction generators in variable-speed wind turbine systems. In: 2015 International Conference on Clean Electrical Power (ICCEP), pp. 406–413. IEEE, Piscataway, NJ (2015)
 29. Ozsoy, E.E., Golubović, E., Sabanovic, A., Gokasan, M.: A stator voltage oriented doubly-fed induction generator control method with a disturbance observer. In: Eurocon 2013, pp. 1102–1107. IEEE, Piscataway, NJ (2013)
 30. Mbukani, M.W.K., Gule, N.: Comparison of high order and second-order sliding mode observer based estimators for speed sensorless control of rotor-tied DFIG. *IET Pow. Electr.* 12(12), 3231–3241 (2019)
 31. Mbukani, M.W.K., Gule, N.: Evaluation of an STSMO-based estimator for power control of rotor-tied DFIG systems. *IET Electr. Power. Appl.* 13(11), 1871–1882 (2019)
 32. Mbukani, M.W.K., Gule, N.: PLL-based sliding mode observer estimators for sensorless control of rotor-tied DFIG systems. *IEEE Trans. Ind. Appl.* 55(6), 5960–5970 (2019)
 33. Chen, F., Jiang, X., Ding, X., Lin, C.: FPGA-based sensor-less PMSM speed control using adaptive sliding mode observer. *IECON 2017-43rd Annual Conference of the IEEE Industrial Electronics Society*, pp. 4150–4154. IEEE, Piscataway, NJ (2017)
 34. Zhu, J., Khayati, K.: A new approach for adaptive sliding mode control: integral/exponential gain law. *Trans. Inst. Meas. Control* 38(4), 385–394 (2016)
 35. Prasad, R.M., Mulla, M.A.: Mathematical modeling and position-sensorless algorithm for stator-side field-oriented control of rotor-tied DFIG in rotor flux reference frame. *IEEE Trans. Energy Conv.* 35(2), 631–639 (2020)
 36. Olubamiwa, O.I., Gule, N.: The optimal design and autonomous testing of a rotor-tied DFIG. In: 2017 IEEE AFRICON, pp. 1378–1383. IEEE, Piscataway, NJ (2017)
 37. Wang, G., Li, Z., Zhang, G., You, Y., Xu, D.: Quadrature PLL-based high-order sliding mode observer for IPMSM sensor-less control with on-line MTPA control strategy. *IEEE Trans. Energy Conv.* 28(1), 214–224 (2013)

How to cite this article: Mbukani, M.W.K., Gule, N.: Assessment of a PLL-ASMO position/speed estimator for sensor-less control of rotor-tied DFIG (RDFIG). *J. Eng.* 2023, 1–14 (2023).
<https://doi.org/10.1049/tjc2.12284>